Original Contribution

Oxidative stress resistance in hippocampal cells is associated with altered membrane fluidity and enhanced nonamyloidogenic cleavage of endogenous amyloid precursor protein

Angela B. Clement [a],*, Gerald Gimpl [b], Christian Behl [a],*

[a] *Institute for Pathobiochemistry, University Medical Center, Johannes Gutenberg University, 55099 Mainz, Germany*
[b] *Department of Biochemistry, Johannes Gutenberg University, 55099 Mainz, Germany*

ARTICLE INFO

ABSTRACT

Reactive oxygen species (ROS) have important roles as signaling molecules in the regulation of a variety of biological processes. On the other hand, chronic oxidative stress exerted by ROS is widely considered a causative factor in aging. Therefore, cells need to be able to adapt to a chronic oxidative challenge and do so to a certain cell-type-specific extent. Recently, we have shown in oxidative-stress-resistant cell lines, $HT22_{H2O2}$ and $HT22_{Glu}$, derived from the neuronal cell line HT22 by chronic exposure to sublethal concentrations of H_2O_2 and glutamate, that, in addition to the known antioxidant defense mechanisms, e.g., activation of antioxidant enzymes or up-regulation of heat-shock proteins, oxidative stress resistance depends on the composition of cellular membranes. Here, we extend our previous investigations and report increased membrane fluidity in $HT22_{H2O2}$ and $HT22_{Glu}$ cells compared to the parental $HT22_{WT}$ cells. The increased membrane fluidity correlates with a redistribution of cholesterol, sphingomyelin, and membrane-associated proteins involved in APP processing between detergent-resistant and detergent-soluble membrane subdomains. The altered membrane properties were associated with drastic changes in the metabolism of the Alzheimer disease-associated amyloid precursor protein (APP), particularly toward enhanced production of soluble APPα, which is a known neuroprotective factor. Thus our -data provide a link between chronic oxidative stress, alterations in membrane fluidity and composition of membrane subdomains, stress adaptation, and APP processing.

© 2010 Elsevier Inc. All rights reserved.

The production of ROS and their detoxification are normal physiological processes, but an imbalance between the production of ROS and their removal may lead to oxidative stress. As inferred from many studies investigating neurodegenerative diseases that are associated with increased generation of oxidative stress, such as Alzheimer disease (AD), Parkinson disease, and amyotrophic lateral sclerosis, the ability to cope with oxidative stress is cell-type specific. In the AD brain, the cerebellum is less affected by neurodegeneration than the hippocampal region or the cortex [1]. Little is known about the physiological mechanisms behind regional sensitivity to oxidative stress. The cell-type-specific equipment of antioxidant defense systems, such as antioxidant molecules and heat-shock proteins, seems to contribute to a distinct cellular response to oxidative stress.

Recently, we have shown that the lipid composition of cellular membranes is an additional important determinant of cell-type-specific stress resistance [2]. We have employed a neuronal cell culture model based on the hippocampal cell line HT22, which was exposed to a mild oxidative stress by chronic exposure to sublethal concentrations of H_2O_2 or glutamate, resulting in the production of $HT22_{H2O2}$ and $HT22_{Glu}$ cells, respectively, which are more stress resistant to further exposure to these treatments than the parental $HT22_{WT}$ cells [3]. In HT22 cells, glutamate elicits oxidative stress via its inhibitory action on a cysteine–glutamate antiporter, which results in the depletion of intracellular cysteine and hence the antioxidant molecule glutathione [4]. Both cell lines, $HT22_{H2O2}$ and $HT22_{Glu}$, are mutually cross-resistant and show similar lipid profiles [3]. Aside from the increased expression of antioxidants and heat shock proteins, these stress-resistant cells are characterized by a different cholesterol and sphingomyelin metabolism and by an increase in autophagic activity compared to the parental $HT22_{WT}$ cells. Treatment of vulnerable $HT22_{WT}$ cells with a sphingomyelinase inhibitor to increase cellular sphingomyelin levels enhanced stress resistance, confirming the hypothesis that alterations in the cellular lipid balance affect vulnerability to oxidative stress [2]. To deepen our understanding of the reciprocal influence of the

functional network of cellular lipids and oxidative stress, we focused our investigations on differences in membrane fluidity and in the composition of lipid rafts of oxidative-stress-resistant and vulnerable HT22 cells. Lipid rafts are cholesterol- and sphingolipid-rich detergent-resistant membrane subdomains (DRMs). By their dynamic recruitment of transmembrane or membrane-associated proteins, DRMs regulate many physiological processes, such as the activation of signaling pathways or the enzymatic processing of membrane-bound proteins, which may modulate cellular stress resistance. In addition to analyzing the distribution of cholesterol and sphingomyelin between DRMs and non-DRMs, we particularly investigated the localization of proteins involved in the metabolism of APP because APP processing is known to be strongly influenced by alterations in the lipid environment and several studies indicate a role for APP in antioxidant responses [5,6]. It has been demonstrated that higher membrane fluidity favors the nonamyloidogenic α-secretase cleavage of APP, whereas lower membrane fluidity is associated with preferential β-secretase cleavage, leading to an increase in toxic Aβ fragments [7]. In addition, depending on whether APP is cleaved via the amyloidogenic or the nonamyloidogenic process, APP fragments themselves are known to induce oxidative stress or to act neuroprotective, respectively [8].

Materials and methods

Reagents

The following commercial antibodies were used for Western blotting: polyclonal anti-BACE-1 (Abcam); monoclonal anti-caveolin-1 (Transduction Laboratories); polyclonal A8717 (Sigma) against the C-terminus of APP; monoclonal 22C11 (Chemicon), which is directed against amino acids 66–81 of the amino-terminus of APP; polyclonal anti-nicastrin (Sigma); and monoclonal anti-tubulin and polyclonal anti-actin (Sigma). Polyclonal anti-presenilin-1 antibodies 3108 and 3110 were raised to the loop domain (amino acids 263–407) of presenilin-1 (PS-1), as described previously [9]. Polyclonal antibody 1704, which was raised against the last 15 amino acids of the cytoplasmic domain of human low-density lipoprotein receptor-related protein (LRP), has been described previously [10,11]. Secondary donkey anti-mouse and donkey anti-rabbit horseradish peroxidase-conjugated antibodies were from Dianova. Biotinylated anti-rabbit Ig and the ABC kit (used to enhance the BACE-1 signals) were obtained from Vector Laboratories. All other biochemicals used were obtained from regular commercial sources unless stated otherwise.

Cell culture

The initial isolation and maintenance of $HT22_{WT}$, $HT22_{H2O2}$, and $HT22_{Glu}$ cells have been described previously [2,3]. Cells were cultured in DMEM containing 10% fetal calf serum, 1 mM sodium pyruvate, and $1\times$ penicillin/streptomycin from Invitrogen. To maintain the oxidative stress resistance, 450 μM H_2O_2 (Sigma) or 40 mM glutamate (Sigma) was added twice a week to $HT22_{H2O2}$ or $HT22_{Glu}$ cells, respectively. Before experiments, cells were cultured for 10 days without toxins and medium was changed daily to remove residual toxins.

For inhibition of γ-secretase activity, cells were treated for 30 h at 37°C with 1.5 μM γ-secretase inhibitor L685,458 (Sigma) in normal culture medium.

Measurement of membrane fluidity

Five hundred microliters of a 3×10^6 cells/ml suspension in PBS was mixed with 500 μl of the fluorophore 1-(4-trimethylammonium-phenyl)-6-phenyl-1,3,5-hexatriene p-toluene sulfonate (TMA-DPH; 1 μM in PBS) immediately before measurement. This reporter fluorophore incorporates very rapidly into the plasma membrane and remains localized there for at least 25 min [12]. The anisotropy measurements were performed for 3 min at 37°C on a QuantaMaster spectrofluorimeter (PTI, Toronto, ON, Canada). Placed in a 1-ml thermostated cuvette, the sample was excited at 365 nm, and emission was measured at 420 nm using slit widths of 5 nm. A cutoff filter (GG395) was placed in front of the emission filter to reduce light scattering. The steady-state fluorescence anisotropy, r, was determined according to

$$r = (I_{VV} - I_{VH}G) / (I_{VV} + I_{VH}G),$$

where I_{VV} and I_{VH} are the fluorescence intensities observed with the excitation polarizer in the vertical position and the analyzing emission polarizer in both the vertical (I_{VV}) and the horizontal (I_{VH}) configurations. The factor G was used to correct for the unequal transmission of differently polarized light. Because of its cationic moiety, TMA-DPH is anchored only in the outer leaflet of the plasma membrane. Because the rate of internalization of TMA-DPH is very slow, the measured anisotropy values represent organization in the cellular plasma membranes [12].

Preparation of DRMs

Cells grown to 70% confluency in a 10-cm dish were washed twice with ice-cold PBS, scraped in 1 ml PBS, collected by centrifugation at 1000 g for 5 min at 4 °C, and resuspended in 300 μl lysis buffer (50 mM Tris–Cl, pH 7.4, 150 mM NaCl, 5 mM EDTA, 1 mM phenylmethylsulfonyl fluoride, 20 mM CHAPS). After incubation on ice for 30 min the cell lysate was mixed with 300 μl 80% sucrose solution (in lysis buffer without CHAPS) to give a 40% sucrose-containing solution. The 40% sucrose solution was overlaid by a step gradient of 1.3 ml 30% sucrose and 250 μl 5% sucrose. By centrifugation for 120 min at 200,000 g at 4°C, CHAPS-insoluble, lipid-rich, low-density membrane microdomains (floating at the interface between 5 and 30% sucrose) were separated from high-density membrane fractions (collecting at the bottom of the gradient). Ten fractions were collected from the top and 20 μl of each fraction was analyzed by Western blot analysis. For the determination of free unesterified cholesterol and sphingomyelin 50 and 100 μl of each fraction was analyzed using the Amplex red cholesterol assay kit or the sphingomyelinase assay kit, respectively (Invitrogen).

Western blot analysis

Cells from 70% confluent 10-cm dishes were cultured for 24 h. The cells were washed twice and scraped into ice-cold PBS. After centrifugation at 1000 g for 5 min at 4°C the cells were lysed in a buffer containing 62.5 mM Tris, pH 6.8, 2% SDS, 10% sucrose, 5 mM EDTA supplemented with phenylmethylsulfonyl fluoride (5 mg/ml) and aprotinin (1 μg/ml). Extracts were sonicated briefly and denatured for 5 min at 95°C. Protein concentrations of the samples were determined using the BCA kit (Pierce) with bovine serum albumin as a standard. Thirty micrograms of protein/lane was separated by SDS–PAGE on 4–12% Bis–Tris-gradient gels (Invitrogen) and analyzed by Western blotting with the appropriate antibodies. For the determination of soluble (s) APP, gel loading of medium samples was normalized to the corresponding cell extracts. sAPP was detected by the monoclonal antibody 22C11. Western blot signals were quantified by AIDA Image software. Actin or tubulin was used to ensure equal protein loading of cell lysate samples.

Cell surface biotinylation

Cells from 70% confluent cultures were washed twice with ice-cold PBS, chilled on ice for 5 min to block endocytosis, and biotinylated
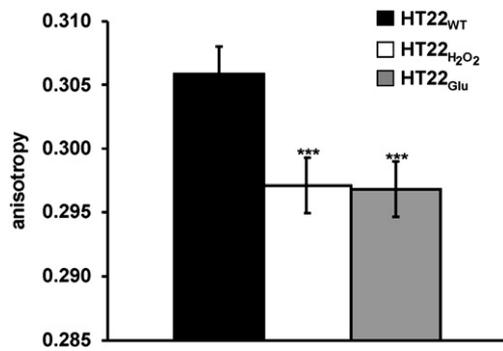
Fig. 1. Plasma membrane fluidity is increased in HT22$_{H2O2}$ and HT22$_{Glu}$ cells. Anisotropy measurements using TMA-DPH as a fluorescent probe that intercalates rapidly and stably into the plasma membrane served to estimate plasma membrane fluidity of HT22$_{WT}$, HT22$_{H2O2}$, and HT22$_{Glu}$ cells. Note that the fluorescence anisotropy values are inversely proportional to membrane fluidity. Anisotropy values are depicted as mean values ± SD ($n = 5$). ***$p < 0.005$ compared to HT22$_{WT}$.

with 1 mg EZ-Link Sulfo-NHS-LC-Biotin (Pierce) in 2 ml PBS/culture dish (100-mm diameter) for 1 h at 4°C. After cell surface biotinylation, the cells were washed twice with ice-cold PBS and subsequently incubated on ice with 50 mM glycine/PBS for 15 min to quench the biotinylation reaction. Subsequently, cells were lysed in 500 μl of buffer A (for composition see below) and left on ice for 60 min. After a centrifugation step (10 min, 25,000 g, 4°C) to remove nonsolubilized material, the cell lysates were adjusted to the same protein concentration (120 μg/ml) by addition of buffer A so that the total volume was 500 μl. To each lysate, 60 μl of NeutrAvidin beads (Pierce) was added. After incubation for 1 h at 4°C the supernatant was removed and kept for SDS–PAGE analysis. The beads were washed twice with each buffer, B, C, and D, and then boiled in sample buffer for SDS–PAGE and subjected to Western blot analysis with the 22C11 antibody against APP. The buffer compositions were as follows: buffer A, 50 mM Tris–Cl, pH 7.4, 150 mM NaCl, 10 mM EDTA, 1% NP-40, 0.1% sodium desoxycholate; buffer B, 10 mM Tris–Cl, pH 7.4, 150 mM NaCl, 2 mM EDTA, 0.2% NP-40; buffer C, 10 mM Tris–Cl, pH 7.4, 500 mM NaCl, 2 mM EDTA, 0.2% NP-40; buffer D, 10 mM Tris–Cl, pH 7.4.

Determination of γ-secretase activity

Enzymatic activity of γ-secretase in total cell extracts was analyzed using a γ-secretase activity kit (R&D Systems, Wiesbaden-Nordenstadt, Germany) following the manufacturer's instructions. For the determination of γ-secretase activity, the same amounts of cellular protein were used.

Statistical analysis

Statistical significance was determined by the unpaired two-tailed Student *t* test using the SigmaStat software; significance was set at $p ≤ 0.05$ and $p ≤ 0.005$.

Results

Plasma membrane fluidity is increased in HT22$_{H2O2}$ and HT22$_{Glu}$ cells

The previously reported differences in lipid composition between oxidative-stress-resistant HT22$_{H2O2}$/HT22$_{Glu}$ cells and HT22$_{WT}$ cells [2] are probably reflective of differences in membrane fluidity, which will certainly affect the cellular metabolism. To measure plasma membrane fluidity we examined the steady-state fluorescence anisotropy using the dye TMA-DPH. Anisotropy values are inversely proportional to the degree of membrane fluidity. Interestingly, in contrast to the reported decrease in membrane fluidity in cells exposed to acute oxidative stress [13–15], a significant increase in

plasma membrane fluidity was found for HT22$_{H2O2}$ and HT22$_{Glu}$ cells, which were generated by chronic exposure to oxidative stress, compared to HT22$_{WT}$ cells (Fig. 1).

Cholesterol and proteins contributing to APP processing migrate toward the non-DRM fraction whereas sphingomyelin levels increase in DRMs of stress-resistant cells

The observed increase in membrane fluidity in HT22$_{H2O2}$ and HT22$_{Glu}$ cells suggests that the actual localization and/or distribution of lipids and membrane-associated proteins might be altered compared to HT22$_{WT}$ cells. We therefore analyzed the composition of different membrane regions, DRMs and non-DRMs, in all cell lines. Thereby we concentrated on the localization of cholesterol, sphingomyelin, and membrane-associated proteins involved in APP processing. Cholesterol is a major component of DRMs, in which amyloidogenic APP processing takes place after APP has been endocytosed, whereas processing of APP to the nonamyloidogenic form by α-secretase has been reported to take place in non-DRMs of the plasma membrane [16–18]. To investigate whether cholesterol distribution between the DRM and the non-DRM fractions is changed in HT22$_{H2O2}$ and HT22$_{Glu}$ versus HT22$_{WT}$ cells, we determined the relative amount of cholesterol in DRMs of these cell lines. DRMs were isolated by extracting cells with 20 mM CHAPS and subsequent sucrose density gradient ultracentrifugation. The cholesterol content in DRMs of HT22$_{H2O2}$ and HT22$_{Glu}$ cells was significantly reduced, whereas it was increased in the non-DRM fraction compared to HT22$_{WT}$ cells (Fig. 2A). In contrast, the relative proportion of sphingomyelin was increased in DRMs and decreased in non-DRMs of the stress-resistant cells (Fig. 2B). Furthermore, we studied the localization of caveolin-1, as a typical DRM marker; of APP; and of
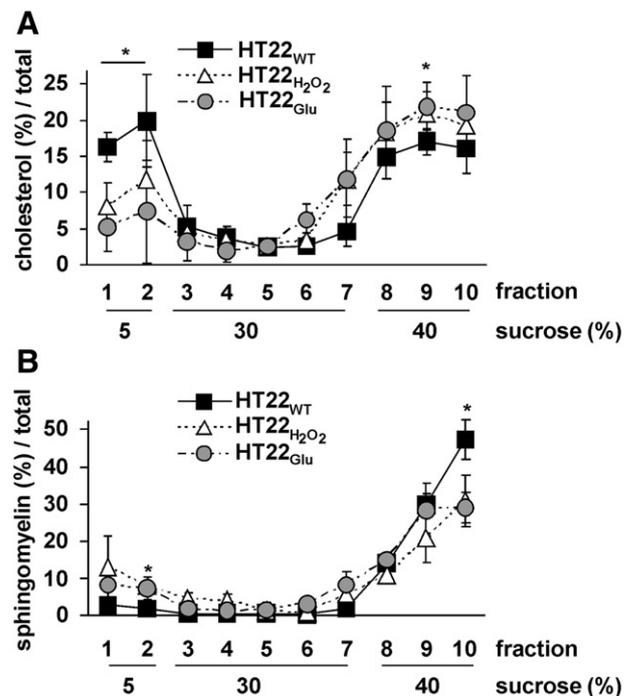

Fig. 2. DRM composition is changed in HT22$_{H2O2}$ and HT22$_{Glu}$ cells compared to HT22$_{WT}$ cells. The percentage of (A) free cholesterol and (B) sphingomyelin was estimated in DRMs, which were prepared by extraction of HT22$_{WT}$, HT22$_{H2O2}$, and HT22$_{Glu}$ cells using 20 mM CHAPS (30 min, 4°C) and subsequent sucrose density gradient centrifugation. Cholesterol and sphingomyelin were determined, using commercially available kits, in 50 and 100 μl of each fraction, respectively. The sum of free cholesterol or sphingomyelin in all fractions after sucrose density gradient centrifugation was considered as 100%. Columns represent mean values ± SD from three independent experiments. *$p < 0.05$ for HT22$_{WT}$ vs HT22$_{H2O2}$ and HT22$_{Glu}$ cells.

several proteins that play important roles in APP processing and clearance, such as nicastrin, PS-1, BACE-1, and LRP. In HT22$_{WT}$ cells we found a substantial fraction of caveolin-1, nicastrin, LRP, and PS-1 in DRMs (at the interface between 5 and 30% sucrose, Fig. 3, left). A majority of cellular proteins were detected in the non-DRM (40% sucrose) fractions at the bottom of the gradient as shown by Coomassie staining of the proteins after gel electrophoresis (Fig. 3). This clearly demonstrated that caveolin-1, nicastrin, LRP, and PS-1 are truly enriched in the DRM fraction. In comparison to the above-mentioned proteins, only a minor population of BACE-1 and full-length APP resided in DRMs in all investigated cell lines (Fig. 3). In all cells, BACE-1 occurred mainly as a dimer. Dimerization of BACE-1 has been reported recently for several tissues and cell lines and seems to facilitate substrate binding and cleavage [19,20].

Importantly, in HT22$_{H2O2}$ and HT22$_{Glu}$ cells the relative amounts of all analyzed proteins in DRMs were reduced compared to those in HT22$_{WT}$ cells, suggesting a general disintegration of CHAPS-resistant DRMs in stress-resistant cells (Fig. 3, middle and right), which would also point to a higher membrane fluidity.

APP processing is shifted toward the nonamyloidogenic pathway in HT22$_{H2O2}$ and HT22$_{Glu}$ cells

The increased plasma membrane fluidity and the observed shift in cholesterol, APP, and other AD-associated APP-processing proteins to non-DRMs led us to hypothesize that α-secretase activity should be altered in oxidative-stress-resistant cells compared to stress-sensitive cells. Western blot analysis using antibodies that are directed against the C-terminus of APP showed the three isoforms of full-length APP (APP$_{fl}$) in neuronal cells: the mature, N- and O-glycosylated, and the immature forms of APP$_{695}$, APP$_{751}$, and APP$_{770}$ (Figs. 3 and 4A, second row from top). Comparison of APP$_{fl}$ protein in total lysates of stress-resistant and vulnerable cells showed clearly a reduction in the highest glycosylated APP$_{fl}$ protein in HT22$_{H2O2}$ and HT22$_{Glu}$ cells, reasoned from the reduced appearance of the highest of the three bands compared to HT22$_{WT}$ cells (Fig. 4A, second row from top). Relative to the APP$_{fl}$ protein, levels of sAPP released into the medium by HT22$_{H2O2}$ and HT22$_{Glu}$ cells increased compared to HT22$_{WT}$ cells (detected by N-terminal APP antibody 22C11, Fig. 4A, top row). Because Western blot analysis by antibodies directed against the C-terminus of APP gave a strong signal for CTFα, but did not detect any CTFβ in these cell lines (Fig. 4A, third row from top), the increase in sAPP in the medium of HT22$_{H2O2}$ and HT22$_{Glu}$ cells reflects an increase in α-secretase-cleaved APP, sAPPα.

APP shedding by α-secretase occurs mainly at the cell surface [17]. The observed increase in sAPPα prompted us to examine whether stress-resistant cells have more APP localized at the plasma membrane than the vulnerable parental cells. Indeed, we observed a strong increase in cell surface-biotinylated APP in HT22$_{H2O2}$ cells compared to HT22$_{WT}$ cells (Fig. 4B). This is in line with the observed enhancement in α-secretase cleavage.
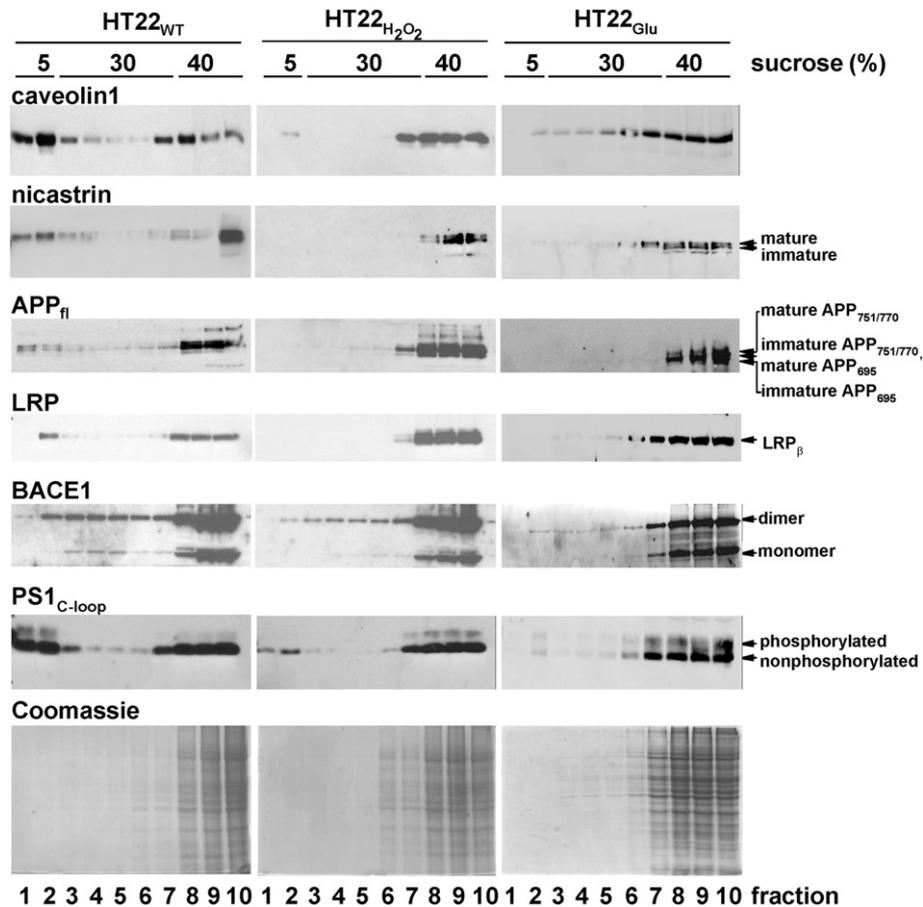

Fig. 3. Proteins contributing to APP processing show reduced levels in DRMs of HT22$_{H2O2}$ and HT22$_{Glu}$ cells compared to HT22$_{WT}$ cells. DRMs from HT22$_{WT}$, HT22$_{H2O2}$, and HT22$_{Glu}$ cells were isolated by extraction of cells with 20 mM Chaps (30 min, 4 °C) and subsequent sucrose density gradient centrifugation. Coomassie staining after gel electrophoresis showed that in all cell types the majority of proteins were localized in the non-DRM 40% sucrose fractions (20 μl of each fraction was loaded per lane). Western blot analysis showed relative enrichment of caveolin-1, a DRM marker, in the DRM fractions (at the interface between 5 and 30% sucrose, left). Partial migration into the DRM fractions was also found for full-length APP (APP$_{fl}$). Note that the APP$_{751}$ and APP$_{770}$ bands migrate together in the chosen gel system. Nicastrin, LRP, BACE-1, and PS-1 were also detected in the DRM fraction in HT22$_{WT}$ cells. In HT22$_{H2O2}$ and HT22$_{Glu}$ cells the amounts of all analyzed proteins in the DRM fractions were reduced compared to HT22$_{WT}$ cells (right). For each protein one representative blot of three independent experiments is shown.
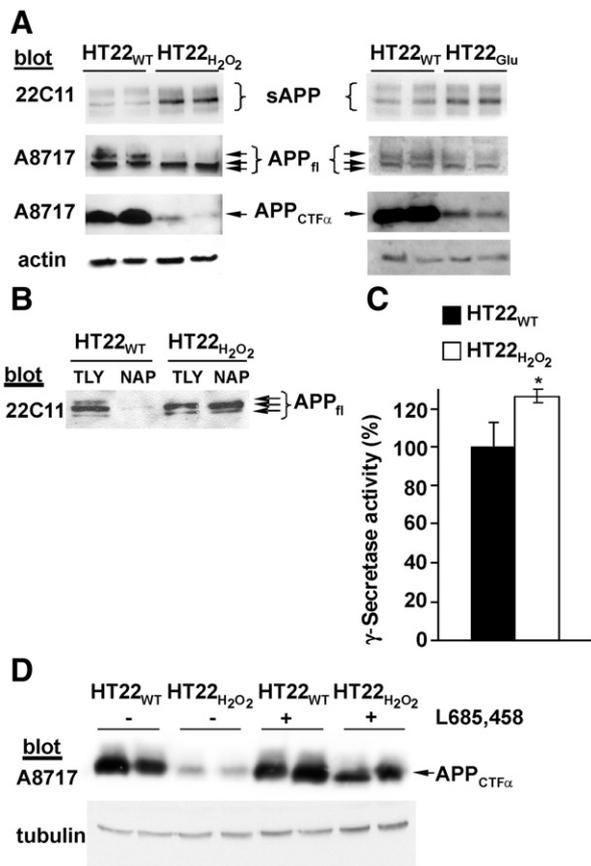
Fig. 4. α- and γ-secretase activity is stimulated in stress-resistant cells. (A) Secretion of sAPP into cell culture medium is increased in $HT22_{H2O2}$ and $HT22_{Glu}$ cells compared to $HT22_{WT}$ cells as revealed by Western blot analysis using the monoclonal antibody 22C11 after protein separation on a 10% Tris–glycine gel (top row, $n=3$). For the analysis of total protein lysates (30 μg/lane) a 4–12% Bis–Tris-gradient gel was used. Western blot analysis employing the polyclonal antibody A8717 showed a decrease in the amount of the highest glycosylated APP_{fl} protein in $HT22_{H2O2}$ and $HT22_{Glu}$ cells compared to $HT22_{WT}$ cells (APP_{751} and APP_{770} bands migrate together in the chosen gel system, indicated by arrows, second row, $n=3–5$). In addition, the C-terminal fragment of APP ($APP_{CTFα}$) was strongly reduced in $HT22_{H2O2}$ and $HT22_{Glu}$ cells (third row, $n=3–5$). No $APP_{CTFβ}$ was detected. (B) Cells were surface biotinylated and lysed and biotinylated proteins were precipitated by NeutrAvidin beads. Subsequent Western blot analysis with anti-APP antibody 22C11 was performed using 10 μg/lane of total lysates (TLY) and NeutrAvidin precipitates (NAP) from 30 μg of the total lysates. The amount of plasma membrane APP_{fl} was increased in $HT22_{H2O2}$ cells ($n=3$). (C) γ-Secretase activity assay demonstrated significantly higher γ-secretase activity in $HT22_{H2O2}$ cells compared to $HT22_{WT}$ cells. Diagram shows means ± SEM of three independent experiments performed in quadruplicate. *$p<0.05$. (D) Treatment with the γ-secretase inhibitor L685,458 (1.5 μM for 30 h) induced a strong increase in $APP_{CTFα}$ in $HT22_{H2O2}$ cells, but not in $HT22_{WT}$ cells. Actin or tubulin served as loading control for the analysis of total lysates as indicated.

Levels of the C-terminal fragment of APP, which results from α-secretase cleavage, were not increased as we would have expected from enhanced α-secretase cleavage, but markedly reduced in $HT22_{H2O2}$ and $HT22_{Glu}$ cells (Fig. 4A, third row). This indicates increased processing of $APP_{CTFα}$ by γ-secretase. Measurement of γ-secretase activity showed indeed enhanced activity in $HT22_{H2O2}$ cells (Fig. 4C). In concert with this, treatment for 30 h with the highly specific transition-state analog inhibitor of γ-secretase, L-685,458, led to accumulation of $APP_{CTFα}$ in $HT22_{H2O2}$ cells (Fig. 4D). In $HT22_{WT}$ cells, the $APP_{CTFα}$ level did not change after treatment with L-685,458. We assume that the activity of γ-secretase in these cells is very low and further inhibition does not visibly increase the amount of $APP_{CTFα}$ above the already high levels. Direct measurement of the γ-secretase-generated intracellular APP fragment (AICD) were not possible given that the endogenous levels of AICD in HT22 cells are difficult to detect.

Discussion

Oxidative stress is generally acknowledged to be associated with AD pathology and has been described as a possible mediator of cell damage in AD. Although the entire brain is subject to an oxidative challenge, certain brain areas are more vulnerable to an oxidative attack than others. Here we searched for the molecular basis of possible endogenous defense mechanisms that distinguish oxidative-stress-resistant cells from cells with a high sensitivity for oxidative stress. For this study we used three neuronal cell lines that differ in their vulnerability to oxidative stress. Recently, we reported that changes in the lipid composition of these cell lines might be one important factor that determines the differential vulnerability to oxidative stress [2]. Now we report that the observed differences in lipid composition result in increased membrane fluidity in stress-resistant cells and correlate with changes in APP processing, shifting APP processing toward an increased release of the neuroprotective sAPPα fragment.

The unique localization of cholesterol enriched in the outer leaflet of the plasma membrane in DRMs suggests that alterations in cellular lipid composition and trafficking due to oxidative stress will affect the activity of membrane-bound proteins involved in APP metabolism. It is important to stress that modulation of total cholesterol by just 10% is sufficient to visibly change DRM composition and membrane fluidity [21]. We have previously shown that cholesterol accumulated in oxidative-stress-resistant cells mainly in lysosomes and not in the plasma membrane [2]. Hence, despite the observed increase in total cholesterol of about 13% in $HT22_{H2O2}$ cells [2], the shift of cholesterol out of the DRM fraction to the non-DRM fraction led us to expect an increase in membrane fluidity. In addition, the observed accumulation of the cholesterol precursors lanosterol and desmosterol [2], which exert weaker condensation effects on lipid acyl chains than cholesterol [22–24], would also suggest a shift to a more disordered plasma membrane. Indeed, plasma membrane fluidity was significantly enhanced in both stress-resistant cell lines compared to $HT22_{WT}$ cells. Increased membrane fluidity might protect cells against oxidative stress, which is known to rigidify membranes [25–27]. This hypothesis is supported by a study showing that the fluidity of synaptic plasma membranes isolated from different rat brain regions proved to be higher in the cerebellum, a brain region that is relatively resistant to oxidative stress, than in the hippocampus or cortex, two relatively vulnerable brain regions [28]. Interestingly, the most fluid synaptic plasma membrane of the cerebellum showed the lowest cholesterol level of the three investigated brain regions.

The observed increase in membrane fluidity is also important with regard to APP processing because higher plasma membrane fluidity due to methyl-β-cyclodextrin-induced cholesterol depletion has been shown to promote α-secretase cleavage of APP and, therefore, the nonamyloidogenic form [29]. Interestingly, in that study Kojro and colleagues also document that replacement of cholesterol by its precursor lanosterol strongly enhances α-secretase activity [29], which is in agreement with our data showing increased lanosterol levels and enhanced α-secretase activity in oxidative-stress-resistant cells. In contrast, cholesterol accumulation in the plasma membrane has been reported to increase the rigidity of the plasma membrane and to decrease α-secretase processing of APP [7].

The observed changes in $HT22_{H2O2}$ and $HT22_{Glu}$ cells toward nonamyloidogenic APP processing to sAPPα will probably contribute to their increased stress resistance. sAPPα is known to act as a neuroprotective cytokine by blocking activation of the proapoptotic c-Jun N-terminal kinase signaling cascade [30,31]. In summary, alterations in the lipid composition of cellular membranes and in membrane fluidity, induced by a permanently increased oxidative microenvironment, are prone to change many different metabolic

processes taking place in distinct membrane compartments (here shown for APP processing), which then may influence the vulnerability of cells to oxidative stressors.

Acknowledgments

References

[1] Hyman, B. T.; Van Hoesen, G. W.; Damasio, A. R.; Barnes, C. L. Alzheimer's disease: cell-specific pathology isolates the hippocampal formation. *Science* **225:**1168–1170; 1984.

[2] Clement, A. B.; Gamerdinger, M.; Tamboli, I. Y.; Lutjohann, D.; Walter, J.; Greeve, I.; Gimpl, G.; Behl, C. Adaptation of neuronal cells to chronic oxidative stress is associated with altered cholesterol and sphingolipid homeostasis and lysosomal function. *J. Neurochem.* **111:**669–682; 2009.

[3] Schafer, M.; Goodenough, S.; Moosmann, B.; Behl, C. Inhibition of glycogen synthase kinase 3beta is involved in the resistance to oxidative stress in neuronal HT22 cells. *Brain Res.* **1005:**84–89; 2004.

[4] Maher, P.; Davis, J. B. The role of monoamine metabolism in oxidative glutamate toxicity. *J. Neurosci.* **16:**6394–6401; 1996.

[5] Schubert, D.; Behl, C. The expression of amyloid beta protein precursor protects nerve cells from beta-amyloid and glutamate toxicity and alters their interaction with the extracellular matrix. *Brain Res.* **629:**275–282; 1993.

[6] Goodman, Y.; Mattson, M. P. Secreted forms of β-amyloid precursor protein protect hippocampal neurons against amyloid β-peptide-induced oxidative injury. *Exp. Neurol.* **128:**1–12; 1994.

[7] Bodovitz, S.; Klein, W. L. Cholesterol modulates alpha-secretase cleavage of amyloid precursor protein. *J. Biol. Chem.* **271:**4436–4440; 1996.

[8] Piccini, A.; Ciotti, M. T.; Vitolo, O. V.; Calissano, P.; Tabaton, M.; Galli, C. Endogenous APP derivatives oppositely modulate apoptosis through an autocrine loop. *Neuroreport* **11:**1375–1379; 2000.

[9] Walter, J.; Grunberg, J.; Capell, A.; Pesold, B.; Schindzielorz, A.; Citron, M.; Mendla, K.; George-Hyslop, P. S.; Multhaup, G.; Selkoe, D. J.; Haass, C. Proteolytic processing of the Alzheimer disease-associated presenilin-1 generates an in vivo substrate for protein kinase C. *Proc. Natl. Acad. Sci. USA* **94:**5349–5354; 1997.

[10] Sisodia, S. S.; Koo, E. H.; Hoffman, P. N.; Perry, G.; Price, D. L. Identification and transport of full-length amyloid precursor proteins in rat peripheral nervous system. *J. Neurosci.* **13:**3136–3142; 1993.

[11] Pietrzik, C. U.; Busse, T.; Merriam, D. E.; Weggen, S.; Koo, E. H. The cytoplasmic domain of the LDL receptor-related protein regulates multiple steps in APP processing. *EMBO J.* **21:**5691–5700; 2002.

[12] Kuhry, J. G.; Fonteneau, P.; Duportail, G.; Maechling, C.; Laustriat, G. TMA-DPH: a suitable fluorescence polarization probe for specific plasma membrane fluidity studies in intact living cells. *Cell Biophys.* **5:**129–140; 1983.

[13] Funk, R. S.; Krise, J. P. Exposure of cells to hydrogen peroxide can increase the intracellular accumulation of drugs. *Mol. Pharmacol.* **4:**154–159; 2007.

[14] Wei, T.; Ni, Y.; Hou, J.; Chen, C.; Zhao, B.; Xin, W. Hydrogen peroxide-induced oxidative damage and apoptosis in cerebellar granule cells: protection by Ginkgo biloba extract. *Pharmacol. Res.* **41:**427–433; 2000.

[15] Yamaguchi, T.; Fujita, Y.; Kuroki, S.; Ohtsuka, K.; Kimoto, E. A study on the reaction of human erythrocytes with hydrogen peroxide. *J. Biochem.* **94:**379–386; 1983.

[16] Chyung, J. H.; Selkoe, D. J. Inhibition of receptor-mediated endocytosis demonstrates generation of amyloid beta-protein at the cell surface. *J. Biol. Chem.* **278:**51035–51043; 2003.

[17] Ehehalt, R.; Keller, P.; Haass, C.; Thiele, C.; Simons, K. Amyloidogenic processing of the Alzheimer beta-amyloid precursor protein depends on lipid rafts. *J. Cell Biol.* **160:**113–123; 2003.

[18] Sisodia, S. S. Beta-amyloid precursor protein cleavage by a membrane-bound protease. *Proc. Natl. Acad. Sci. USA* **89:**6075–6079; 1992.

[19] Westmeyer, G. G.; Willem, M.; Lichtenthaler, S. F.; Lurman, G.; Assfalg-Machleidt, I.; Reiss, K.; Saftig, P.; Haass, C. Dimerization of beta-site beta-amyloid precursor protein-cleaving enzyme. *J. Biol. Chem.* **279:**53205–53212; 2004.

[20] Schmechel, A.; Strauss, M.; Schlicksupp, A.; Pipkorn, R.; Haass, C.; Bayer, T. A.; Multhaup, G. Human BACE forms dimers and colocalizes with APP. *J. Biol. Chem.* **279:**39710–39717; 2004.

[21] Gaus, K.; Gratton, E.; Kable, E. P.; Jones, A. S.; Gelissen, I.; Kritharides, L.; Jessup, W. Visualizing lipid structure and raft domains in living cells with two-photon microscopy. *Proc. Natl. Acad. Sci. USA* **100:**15554–15559; 2003.

[22] Megha; Bakht, O.; London, E. Cholesterol precursors stabilize ordinary and ceramide-rich ordered lipid domains (lipid rafts) to different degrees: implications for the Bloch hypothesis and sterol biosynthesis disorders. *J. Biol. Chem.* **281:**21903–21913; 2006.

[23] Miao, L.; Nielsen, M.; Thewalt, J.; Ipsen, J. H.; Bloom, M.; Zuckermann, M. J.; Mouritsen, O. G. From lanosterol to cholesterol: structural evolution and differential effects on lipid bilayers. *Biophys. J.* **82:**1429–1444; 2002.

[24] Cournia, Z.; Ullmann, G. M.; Smith, J. C. Differential effects of cholesterol, ergosterol and lanosterol on a dipalmitoyl phosphatidylcholine membrane: a molecular dynamics simulation study. *J. Phys. Chem. B* **111:**1786–1801; 2007.

[25] Saxena, S.; Srivastava, P.; Kumar, D.; Khanna, V. K.; Seth, P. K. Decreased platelet membrane fluidity in retinal periphlebitis in Eales' disease. *Ocul. Immunol. Inflamm.* **14:**113–116; 2006.

[26] Cazzola, R.; Rondanelli, M.; Russo-Volpe, S.; Ferrari, E.; Cestaro, B. Decreased membrane fluidity and altered susceptibility to peroxidation and lipid composition in overweight and obese female erythrocytes. *J. Lipid Res.* **45:**1846–1851; 2004.

[27] Garcia, J. J.; Reiter, R. J.; Cabrera, J. J.; Pie, J.; Mayo, J. C.; Sainz, R. M.; Tan, D. X.; Qi, W.; Acuna-Castroviejo, D. 5-Methoxytryptophol preserves hepatic microsomal membrane fluidity during oxidative stress. *J. Cell. Biochem.* **76:**651–657; 2000.

[28] Chochina, S. V.; Avdulov, N. A.; Igbavboa, U.; Cleary, J. P.; O'Hare, E. O.; Wood, W. G. Amyloid beta-peptide 1-40 increases neuronal membrane fluidity: role of cholesterol and brain region. *J. Lipid Res.* **42:**1292–1297; 2001.

[29] Kojro, E.; Gimpl, G.; Lammich, S.; Marz, W.; Fahrenholz, F. Low cholesterol stimulates the nonamyloidogenic pathway by its effect on the alpha-secretase ADAM 10. *Proc. Natl. Acad. Sci. USA* **98:**5815–5820; 2001.

[30] Barger, S. W.; Mattson, M. P. Induction of neuroprotective kappa B-dependent transcription by secreted forms of the Alzheimer's beta-amyloid precursor. *Brain Res. Mol. Brain Res.* **40:**116–126; 1996.

[31] Kogel, D.; Schomburg, R.; Copanaki, E.; Prehn, J. H. Regulation of gene expression by the amyloid precursor protein: inhibition of the JNK/c-Jun pathway. *Cell Death Differ.* **12:**1–9; 2005.